A Potential Recoiling Supermassive Black Hole, CXO J101527.2+625911

D.-C. Kim[1], Ilsang Yoon[1], G. C. Privon[2], A. S. Evans[1,3], D. Harvey[4], S. Stierwalt[1], and Ji Hoon Kim[5]

[1] National Radio Astronomy Observatory, 520 Edgemont Road, Charlottesville, VA 22903, USA; dkim@nrao.edu
[2] Instituto de Astrofísica, Facultad de Física, Pontificia Universidad Católica de Chile, Avda. Vicuna Mackenna 4860, Santiago, Codigo Postal: 8970117, Chile
[3] Department of Astronomy, 530 McCormick Road, University of Virginia, Charlottesville, VA 22904, USA
[4] Laboratoire dAstrophysique, EPFL, Observatoire de Sauverny, Chemin des Maillettes, 51, Versoix CH-1290, Suisse, Switzerland
[5] Subaru Telescope, National Astronomical Observatory of Japan, 650 North A'ohoku Place, Hilo, HI 96720, USA

Abstract

We have carried out a systematic search for recoiling supermassive black holes (rSMBH) using the *Chandra* Source and SDSS Cross-Match Catalog. From the survey, we have detected a potential rSMBH, CXO J101527.2 +625911, at $z = 0.3504$. The source CXO J101527.2+625911 has a spatially offset (1.26 ± 0.05 kpc) active SMBH and kinematically offset broad emission lines (175 ± 25 km s^{-1} relative to the systemic velocity). The observed spatial and velocity offsets suggest that this galaxy could be an rSMBH, but we have also considered the possibility of a dual SMBH scenario. The column density toward the galaxy center was found to be Compton thin, but no X-ray source was detected. The non-detection of the X-ray source in the nucleus suggests that either there is no obscured actively accreting SMBH or that there exists an SMBH, but it has a low accretion rate (i.e., a low-luminosity AGN (LLAGN)). The possibility of the LLAGN was investigated and found to be unlikely based on the Hα luminosity, radio power, and kinematic arguments. This, along with the null detection of an X-ray source in the nucleus, supports our hypothesis that CXO J101527.2+625911 is an rSMBH. Our GALFIT analysis shows the host galaxy to be a bulge-dominated elliptical. The weak morphological disturbance and small spatial and velocity offsets suggest that CXO J101527.2+625911 could be in the final stage of a merging process and about to turn into a normal elliptical galaxy.

Key words: quasars: supermassive black holes

1. Introduction

Galaxy interactions play an important role in galaxy evolution. The interactions enhance starburst activity (Larson & Tinsley 1978; Joseph et al. 1984; Sanders et al. 1988), induce starburst and active galactic nuclei (AGN) feedback (Lehnert & Heckman 1996; Heckman et al. 2000; Rupke et al. 2002), enrich the intergalactic medium with outflows (Nath & Trentham 1997; Scannapieco et al. 2002), and aid the formation and growth of stellar bulges and supermassive black holes (SMBHs) (Kormendy & Richstone 1995; Magorrian et al. 1998; Ferrarese & Merritt 2000; Gebhardt et al. 2000; Tremaine et al. 2002; Marconi & Hunt 2003; Hopkins et al. 2005; Kormendy & Ho 2013). When two SMBHs coalesce at the final stage of a galaxy interaction, *a merged SMBH* can recoil from the host galaxy as a result of anisotropic emission of the gravitational waves (Peres 1962). Recent simulations of merging black holes predict that the merged SMBH can attain a kick velocity of a few hundred to a few thousand km s^{-1} depending on mass ratios, spin magnitudes, and spin orientations of the merging SMBHs (Campanelli et al. 2007, Schnittman 2007; Baker et al. 2008; Lousto & Zlochower 2011; Blecha et al. 2016). If the merging SMBHs are of equal mass and spin fast, and if their spins are aligned along the orbital plane (superkick configuration), recoil velocities as high as 4000 km s^{-1} (Campanelli et al. 2007) to 5000 km s^{-1} (Lousto & Zlochower 2011) can be reached, and the recoiling SMBH (hereafter rSMBH) will eventually escape from the host galaxy (i.e., Merritt et al. 2004).

The recoiling supermassive black hole (rSMBH) carries it the broad-line region (BLR) along with it and leaves the stellar nucleus behind; it can be observable for tens of Myr as an offset AGN (Madau & Quataert 2004; Loeb 2007,

Blecha et al. 2011, 2016). We therefore expect two observational characteristics: (i) the rSMBH could be observed spatially offset with respect to the stellar center of the host galaxy, and (ii) the broad emission lines could have a measurable velocity offset with respect to the systemic velocity. So far, there have been more than a dozen reports of rSMBH candidates. Some examples of rSMBH candidates are SDSS J092712.65+294344.0 (Komossa et al. 2008), SDSS J105041.35+345631.3 (Shields et al. 2009), M87 (Batchedor et al. 2010), QSO E1821+643 (Robinson et al. 2010), CXOC J100043.1+020637 (Civano et al. 2010), CXO J122518.6 +144545 (Jonker et al. 2010), a half-dozen SDSS QSOs (Eracleous et al. 2012), 10 nearby core elliptical galaxies (Lena et al. 2014), NGC 3115 (Menezes et al. 2014), 5 SDSS AGNs (Comerford et al. 2015), and 26 SDSS QSOs (Kim et al. 2016). Except for CXOC J100043.1+020637, most of the rSMBH candidates described to date either have a spatial offset or a velocity offset, but not both. The source CXOC J100043.1 +020637 has two compact sources separated by ∼2.5 kpc and has a velocity offset of ∼1200 km s^{-1} (Civano et al. 2010). *Chandra* observations find that the southeastern source, which has a point-like morphology typical of a bright AGN, is responsible for the whole X-ray emission in this system (Civano et al. 2012). The northwestern source has a more extended profile in the optical band, with a scale length of ∼0.5 kpc. Recent 3 GHz Karl G. Jansky Very Large Array (VLA) observations find that the entire observed 3 GHz radio emission can be associated with the southeastern nucleus (Novak et al. 2015). The observations favored an explanation within the rSMBH picture, but the presence of an obscured and radio-quiet SMBH in the northwestern source is not ruled out (i.e., Blecha et al. 2013; Wrobel et al. 2014).

Here, we report an analysis of optical imaging and spectroscopy, as well as X-ray data, of CXO J191527.2+625911 and show that it is one of the best rSMBH candidates to date. The paper is divided into four sections. In Section 2 we describe the detection of CXO J101527.2+625911 from the systematic search for rSMBH. The discussion is presented in Section 3, and a summary of the paper is presented in Section 4. Throughout this paper, we adopt a cosmology $H_0 = 70\,\mathrm{km\,s^{-1}\,Mpc^{-1}}$, $\Omega_M = 0.3$, and $\Omega_\Lambda = 0.7$.

## 2. Detection of a Potential rSMBH, CXO J101527.2+625911

We have conducted a systematic search for rSMBHs from the *Chandra* Source Catalogs (CSC)—Sloan Digital Sky Survey (SDSS) Cross-Match Catalog (Evans et al. 2010; Rots & Budavári 2011). The CSC-SDSS Cross-Match Catalog (CSC-SDSS CC) contains a total of 19,275 sources of which SDSS images for all and SDSS spectra for a significant part of the sources exist, enabling us to identify both spatial and velocity offsets of the rSMBH candidates. Another advantage of using the CSC-SDSS CC is that all entries are X-ray sources, many of which are AGNs. In addition to the SDSS images, we have searched the *Hubble Space Telescope* (*HST*) for images that contain sources in the CSC-SDSS CC. The initial selection of possible images containing the rSMBH candidate was made by searching the *HST* archive for WFPC1/2, NICMOS, ACS, and WFC3 images with central coordinates within a 2.′5 radius of the CSC-SDSS CC position for each source. This selection criterion returned matches for 3873 sources. Each *HST* image was then examined to see if it contained the optical/near-infrared counterpart of the CSC-SDSS CC sources. We found that 2542 of the sources have *HST* imaging data. The next step in the selection process was to examine the *HST* and SDSS images in order to determine the morphology of the host galaxy. Host galaxies with overlapping nuclei or double nuclei within a half-radius of a single galaxy were selected. However, if the galaxies are apparently interacting or strongly disturbed, we excluded them since we cannot accurately determine the center of these galaxies. We then inspected the SDSS spectra of the selected rSMBH candidates. In cases in which these sources have broad lines in the spectra and only a single set of narrow emission lines, we performed a spectral decomposition to determine whether any broad-line velocity offset relative to the systemic velocity was observed. For the spectral decomposition, we used the IRAF/Specfit package with three component fits in the Hα region: (i) power-law continuum, (ii) broad emission line, and (iii) narrow emission line. We applied a single Lorentzian or a single Gaussian profile for the Hα broad-line component and a single Gaussian profile for the Hα and [N II] narrow line components. The same Gaussian line widths were used for the narrow emission lines of Hα and [N II], and a fixed value of 1/3 was used for the [N II]6548 to [N II]6583 line ratio. In this process, we excluded sources with two sets of narrow emission lines since they are most likely interacting galaxies or dual SMBHs.

A potential rSMBH candidate, CXO J101527.2+625911 ($z = 0.3504$), was discovered in this process. In the *HST*/ACS I-band (F775W) image (Treu et al. 2007) in Figure 1(a), CXO J101527.2+625911 looks more like an E/S0 galaxy with tidal features on the east side (thick tidal tail) and west side (thin spiral-like structure). In the center of the galaxy, two nuclei are clearly visible, one in the north and the other in the south. The two nuclei are more prominent in the zoom-in image with the contour plot overlaid (Figure 1(b)): a southern nucleus and a much brighter (∼6×) northern nucleus. The position of the southern nucleus is near the center of the galaxy, and the northern nucleus is offset from the center. In order to determine the relative positions of each nucleus within the host galaxy, we performed an ellipse fitting. Before the ellipse fitting, we subtracted the northern nucleus component since it is apparently offset from the center of the galaxy and will produce an incorrect centroid. The ellipse fitting was made within the circled region in Figure 1(a) using the IRAF/Ellipse package (we excluded the disturbed and asymmetric part of the galaxy outside of the circled region since it will produce an incorrect centroid). The ellipse fitting produces center positions of the fitted ellipses as a function of radius. We calculated the positional offsets of the center of each ellipse with respect to the center of the southern nucleus. If the southern nucleus is the true host galaxy center, we will see a small or no offset. The result is plotted in Figure 1(c), where the magenta circle and green triangle represent the start and end point of the fitting, respectively. The positional offsets range from 0 to 0.′′1 and are less than the FWHM of ACS point-spread function (PSF, 0.′′1–0.′′14). This suggests that the southern nucleus is the center of the host galaxy within the positional uncertainly of the ACS. Hereafter, we call the southern nucleus the nucleus of the host galaxy.

The absolute astrometry of the *HST* images is ∼0.′′3, therefore we cannot measure the positions of the two nuclei better than this limit. To find a more accurate position, we searched the large quasar reference frame (LQRF) catalog (Andrei et al. 2009) and found a quasar position that matches our source. This position and its positional uncertainty (0.′′135) is marked with the white dot and circle, respectively, in Figure 1(b). The magenta plus symbol and circle in the plot represent the position of CXO J101527.2+625911 from CSC Ver. 2 and its positional uncertainty (0.′′5), respectively. As shown in the image, the *Chandra* position is closer to the northern nucleus, and the positional uncertainty circles of the LQRF and *Chandra* partly overlap. This suggests that the northern nucleus is the X-ray source (hereafter the offset AGN or offset SMBH). The projected nuclear separation between the offset AGN and the nucleus of the host galaxy is 0.′′26 ± 0.′′01, corresponding to a physical scale of 1.26 ± 0.05 kpc.

To estimate the recoil velocity, a spectral decomposition was performed for the Hβ line in the high S/N Keck Low Resolution Imaging Spectrometer (LRIS) spectra (resolution ≃55 km s^{-1}) observed by Woo et al. (2006). The Hα line in the SDSS spectra could be used to measure the recoil velocity, but we decided to use the Keck LRIS spectra since the redshifted Hα line lies at the edge of SDSS spectral coverage and contains noisy signals (Figure 2(a)). For the spectral decomposition, we used the same method as we did for the Hα line. However, the [Fe II] component, which is often found in the QSOs, was not added in the fit since we did not see this line near the Hβ. The result of the spectral decomposition is presented in Figure 2(b), where the black, cyan, blue, green, and red lines represent data, power-law continuum, broad emission line, narrow emission lines, and model (sum of all fitting components), respectively. Vertical dotted and dashed lines represent the line center of the Hβ systemic velocity and the Hβ broad line, respectively, and the systemic velocity ($z = 0.3504$) was measured from the low-ionization forbidden line [S II] $\lambda6716$. The Hβ broad line is
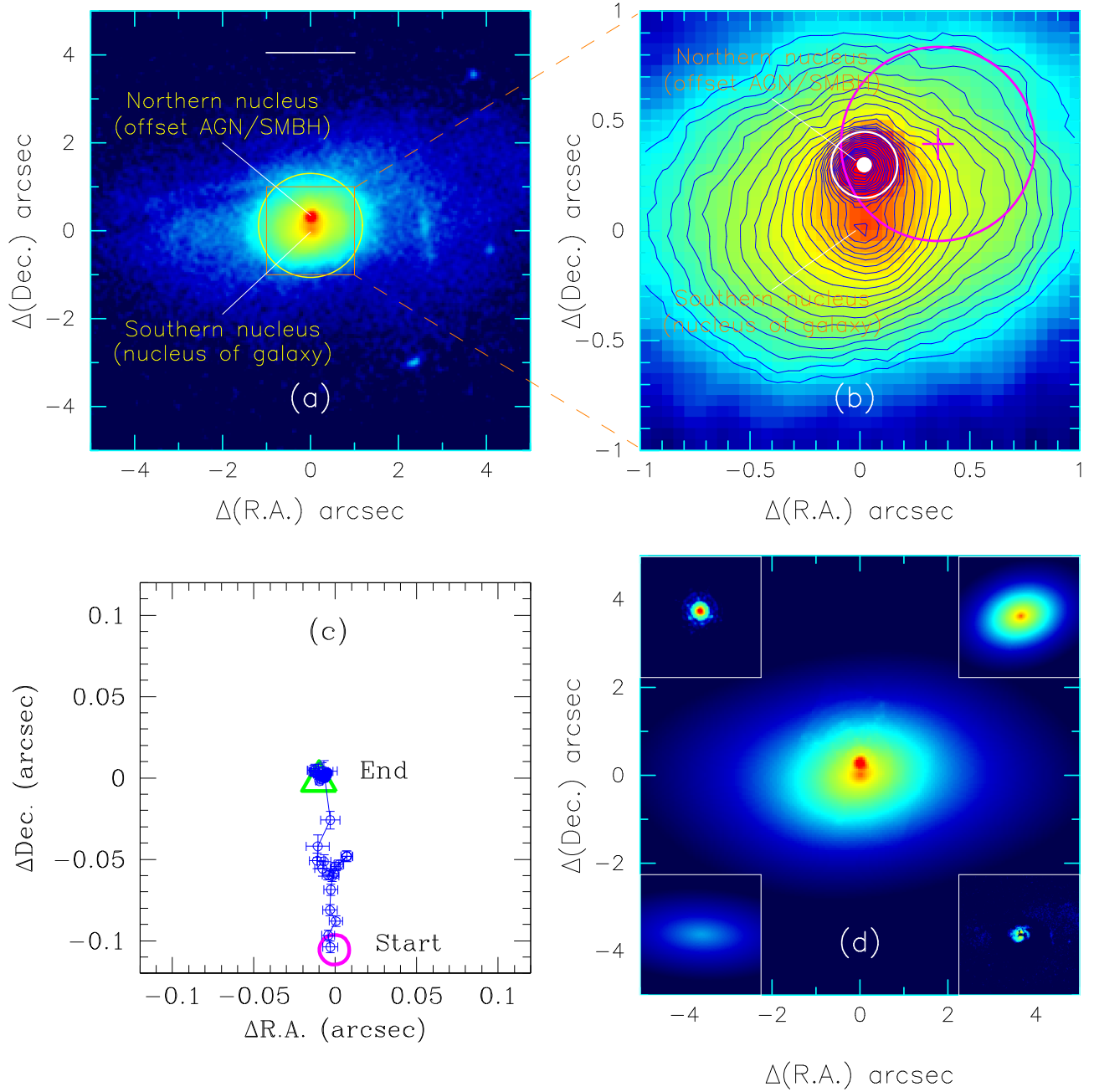
Figure 1. (a) The *HST* ACS image of CXO J101527.2+625911, (b) zoom-in image of the boxed region in panel (a), (c) positional offsets between ellipse-fitting centers and southern nucleus, and (d) model galaxy used in Galfit (upper left: psf, upper right: bulge, lower left: disk, lower right: residual (data-model)). The white dot and circle in panel (b) represent the LQRF quasar position and its positional uncertainty, and the magenta plus symbol and circle represent the location of the *Chandra* X-ray source and its positional uncertainty. Contour levels are spaced log (5) units apart. The horizontal bar in panel (a) represents the 10 kpc physical scale. North is up and east is to the left.

redshifted by 175 ± 25 km s^{-1} relative to the systemic velocity, and its FWHM is 4200 km s^{-1}.

The radio emission from this galaxy was detected ($S_{1.4\,\mathrm{GHz}} = 1.6$ mJy) from the VLA Sky Survey Faint Images of the Radio Sky at Twenty centimetres (FIRST: Becker et al. 1995). The radio luminosity calculated from $L_{1.4\,\mathrm{GHz}} = 4\pi D_l^2 (1+z)^{\alpha-1} S_{1.4\,\mathrm{GHz}}$ with a luminosity distance $D_l = 1859$ Mpc and spectral index $\alpha = 0.7$ is 6.1×10^{23} W Hz^{-1} and places this galaxy in the radio-loud category ($>10^{23}$ W Hz^{-1}). Its q-value (ratio of FIR to radio luminosity, Helou et al. 1985) is 2.08 and similar to the mean value found in quasars, but lower than that found in starburst galaxies (Morić et al. 2010). The X-ray

luminosity of CXO J101527.2+625911 is $L_{0.5-7.0\,\mathrm{keV}} = 2.39 \times 10^{43}$ erg s^{-1} cm^{-2} and about an order higher than that of X-ray-selected broad-line AGNs in a similar redshift range (Suh et al. 2015). The basic properties of CXO J101527.2 +625911 are listed in Table 1.

3. Discussion

3.1. An rSMBH or a Dual SMBH?

Although we have detected both spatial and velocity offsets in CXO J101527.2+625911, this system could be a dual SMBH. If both AGNs in a dual SMBH are actively accreting,
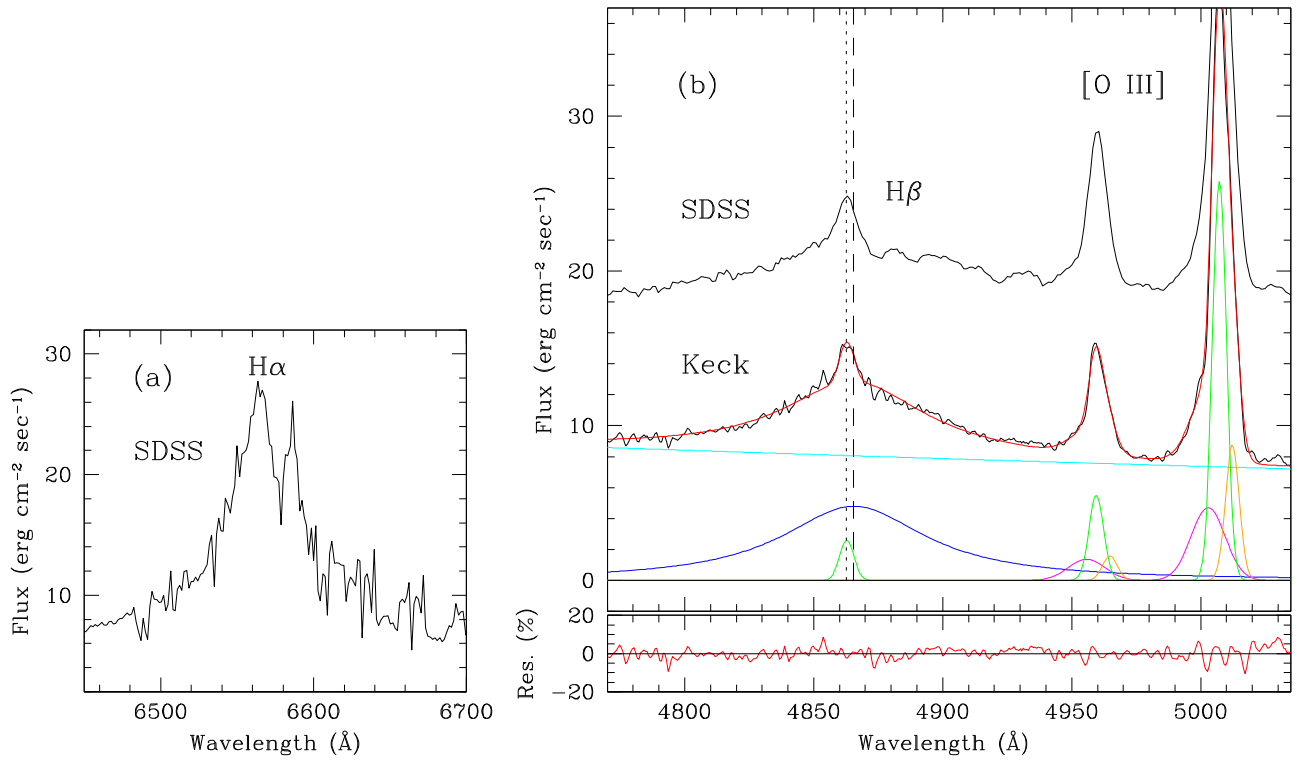
Figure 2. (a) SDSS spectra near the Hα line, (b) result of spectral decompositions of the Hβ line. Dotted and dashed lines represent line centers of the Hβ systemic velocity and the Hβ broad line, respectively. The residual of the fitting (data/model in percentage) is shown in the bottom of the plot. The SDSS spectrum is shown for comparison.

we will observe two sets of shifted narrow and broad lines in the spectra since each AGN has its own BLR and narrow-line region (NLR) and both AGNs will follow the gravitational potential of the host galaxy. If their NLRs are mixed together, we will still observe two sets of shifted broad lines and one set of narrow lines. Detection of only the redshifted broad lines relative to the narrow lines in CXO J101527.2+625911 excludes the scenario of two actively accreting dual SMBHs. The SMBH in the nucleus might be actively accreting, but may be obscured behind gas and dust. X-ray observations will be one of the best methods to detect the obscured SMBHs. From the *Chandra* ACIS-S point source sensitivity limit ($4 \times 10^{-15}\,\mathrm{erg\,cm^2\,s^{-1}}$ in $10^4\,\mathrm{s}$ of exposure time), the Compton thickness (Juneau et al. 2011) in the nucleus can be estimated. If there exists an obscured SMBH in the nucleus of host galaxy, the [O III] flux we have measured will be a combination of emission from the offset SMBH and the obscured SMBH. If we assume that about a half of the [O III] flux comes from the obscured SMBH, the Compton thickness in the nucleus will be Compton thin ($\log(L_{\mathrm{X\text{-}ray}}/L_{[\mathrm{O\,III}]}) = 0.70$). Even if all of the [O III] flux comes from the obscured SMBH, it is still Compton thin ($\log(L_{\mathrm{X\text{-}ray}}/L_{[\mathrm{O\,III}]}) = 0.40$). This means that if there exists an obscured SMBH in the nucleus of the host galaxy and if it is actively accreting, we could have detected the X-ray emission.

The non-detection of the X-ray source in the nucleus suggests that there is no actively accreting SMBH, or that there exists an SMBH, but it has a low accretion rate (i.e., low-luminosity AGN (LLAGN)). The possible existence of the LLAGN in the nucleus was investigated, but was found unlikely based on the following: (i) the typical Hα luminosity and 5 GHz radio power of the LLAGNs are

$L_{\mathrm{H}\alpha} = 1.7 \times 10^{39}\,\mathrm{erg\,s^{-1}}$ and $P_{\mathrm{radio}} = 8.5 \times 10^{19}\,\mathrm{W\,Hz^{-1}}$, respectively (Ho 2008), whereas these quantities are more than 2–3 orders of magnitude larger in CXO J101527.2 +625911 ($L_{\mathrm{H}\alpha} = 3.8 \times 10^{41}\,\mathrm{erg\,s^{-1}}$ and $P_{\mathrm{radio}} = 2.5 \times 10^{23}\,\mathrm{W\,Hz^{-1}}$), and (ii) if there exists an LLAGN in the nucleus, the pair of SMBHs will move in a circular orbit with a rotation velocity of $\sim 500\,\mathrm{km\,s^{-1}}$ (assuming the two black hole masses are similar). However, the measured velocity is only $175\,\mathrm{km\,s^{-1}}$ (it is $\sim 260\,\mathrm{km\,s^{-1}}$ when we consider the inclination angle and the longitude of ascending node). The above X-ray and LLAGN arguments favor an rSMBH scenario rather than a dual SMBH.

It is possible that the source identified as an offset AGN could instead be a bright background source. If a background source is located beween $z = 0.3504$ and $z = 1$, then the comoving volume extended by a solid angle of $0\farcs26$ diameter is $1.3 \times 10^{-3}\,\mathrm{Mpc^3}$. The space density of X-ray sources with $L_{0.5\text{–}7.0\,\mathrm{keV}} = 2.39 \times 10^{43}\,\mathrm{erg\,s^{-1}\,cm^{-2}}$ at $z = 0.3504$ is $5 \times 10^{-5}\,\mathrm{Mpc^{-3}}$ from the X-ray luminosity function of Silverman et al. (2008). If the same source is placed at $z = 1.0$, then the required X-ray luminosity is $L_{0.5\text{–}7.0\,\mathrm{keV}} = 3.05 \times 10^{44}\,\mathrm{erg\,s^{-1}\,cm^{-2}}$ and its space density becomes $8 \times 10^{-6}\,\mathrm{Mpc^{-3}}$. This means that the overlap probability ranges from 6.5×10^{-8} (for a background source at $z = 0.3504$) to 1.1×10^{-8} ($z = 1.0$) and can be ignored.

We find that the narrow-line ratios of [O III]/Hβ and [N II]/Hα are consistent with excitation by an AGN ($\log([\mathrm{O\,III}]/\mathrm{H}\beta) = 1.24$, $\log([\mathrm{N\,II}]/\mathrm{H}\alpha) = -0.10$). The average size (diameter) of the NLR in Seyfert I galaxies is about $D = 4.6\,\mathrm{kpc}$ (Bennert et al. 2006). If we assume that the NLR in our source is similar to this, then the offset AGN is still within the NLR, but not near the center. This means that the

Table 1
Properties of CXO J101527.2+625911

z	Spatial Offset $''$ (kpc)	Velocity Offset km s^{-1}	$L_{0.5-7.0 \text{ keV}}$ log	$L_{1.4 \text{ GHz}}$ log	$\frac{L_{\text{FIR}}}{L_\odot}$ log	σ_v (km s^{-1})	$\frac{M_{\text{BH}}}{M_\odot}$ log	$\frac{L_{\text{bol}}}{L_{\text{Edd}}}$
(1)	(2)	(3)	(4)	(5)	(6)	(7)	(8)	(9)
0.3504	$0''26 \pm 0''01 (1.26 \pm 0.05)$	175 ± 25	43.38	23.79	12.20	190 ± 20	8.21 ± 0.02	0.09 ± 0.01

Note. (1) Redshift. (2) Projected spatial offsets in arcsec and kpc units. (3) Line-of-sight velocity of the Hβ broad-line relative to the systemic velocity. (4) *Chandra* 0.5–7 keV X-ray luminosity in erg s^{-1} cm^{-2} unit. (5) FIRST 1, 4 GHz radio luminosity in Watts Hz^{-1} unit. (6) Far-infrared luminosity. (7) Velocity dispersion. (8) black hole mass estimated with the virial method. (9) Eddington ratio calculated from the virial black hole mass.

offset AGN ionizes NLR gas in a density-stratified NLR environment (ionizes more NLR gas in the center direction and less in the opposite direction). We do not think an obscured (if it exists) nuclear AGN ionized the NLR gas since it is not detected from either the X-ray or the *HST* near-infrared J-band image, even if the nucleus of galaxy is optically thin ($\tau_J = 0.25$).

3.2. Host Galaxy Type

Modeling the galaxy morphology can provide information about the dynamical history of the system. We expect rSMBHs to be in systems with galaxy mergers in their past, and these events will likely be evident in the morphology and light profile of the remnant galaxy. The fitting of the host galaxy requires a careful subtraction of the offset AGN. To generate a realistic PSF at the position of the AGN, we created a TinyTim model of the ACS PSF for the F775W filter for each exposure. Given that the *Hubble* telescope has a time-dependent variability to the PSF that is due to thermal breathing, we estimated the focus position of the space telescope by measuring the shapes of the stars and compared them to 16 different focus positions to determine the best-fitting PSF model (Harvey et al. 2015). With the wavelength and focus position for each exposure, a PSF is generated in pixel space and then combined at the same pixel scale as the data using the publicly available package AstroDrizzle. Two-dimensional galaxy fitting was performed with GALFIT 3.0 (Peng et al. 2010) using a composite model, as shown in Figure 1(d): the PSF model (upper left inset), bulge component (Sérsic index $n = 4$, upper right inset), and disk component (Sérsic index $n = 1$, lower left inset). The fitted host galaxy turned out to be a bulge-dominated (log (bulge/disk) = 1.1) elliptical galaxy. In the residual image (lower right inset), we see an artifact of the imperfect PSF subtraction, but not a sign of interacting galaxy. This suggests that the host galaxy is a merger remnant and that a recoil event could have occurred at the final stage of the tidal interaction.

3.3. M_{BH}–σ Relation

The recoil velocity we measured is only ∼10% of the typical escape velocity in an elliptical galaxy ($v_e \approx$ 1500–2000 km s^{-1}). In this case, the rSMBH will undergo damped oscillations around the center of the host galaxy (Gualandris & Merritt 2008, Blecha et al. 2011). The mass of the oscillating SMBHs may be up to five times lower than their stationary counterparts and could be a source of intrinsic scatter in the SMBH and stellar bulge mass scaling law (Blecha et al. 2011). As shown in Figure 3, our previous study (Kim et al. 2016) supports this claim: the black hole masses (M_{BH}) of the kinematically identified rSMBH candidates (blue circles) are on average

5.2 ± 3.2 times lower than the masses of their SDSS stationary counterparts (green dots). The magenta circle in Figure 3 is the data point of CXO J101527.2+625911, whose black hole mass $M_{BH} = 10^{8.21 \pm 0.02} M_\odot$ was calculated by the virial method (Ho & Kim 2015), and the velocity dispersion σ_* (190 ± 20 km s^{-1}) was estimated from the line width of [S II]6716 (Komossa & Xu 2007). It is interesting to note that CXO J101527.2+625911 does not fit this scenario and more closely follows the M_{BH}–σ_* correlation found in the ellipticals and classical bulges (solid line: Kormendy & Ho 2013). The weak tidal feature, the lack of any anomalies in the residual image in Figure 1(d), and the small spatial (1.25 kpc) and velocity (175 km s^{-1}) offsets may suggest that CXO J101527.2+625911 is in the final stage of damped oscillations and the whole system could turn into a normal elliptical. The Eddington ratio and M_{BH} of CXO J101527.2 +625911 are about six times lower and six times higher than those of rSMBH candidates (Figure 3(b)), respectively, but are similar to values found in X-ray selected broad-line AGNs (Suh et al. 2015). This could indicate that it has almost completed growing its bulge and black hole masses via accretion.

3.4. Star Formation Rate (SFR)

It is suggested that star formation in galaxies is regulated by AGN feedback and outflow (Fabian 2012; Tombesi et al. 2015). If the central AGN is displaced by a recoil event, it will no longer result in quenching, but instead enhance central star formation in the host galaxy (Blecha et al. 2011; Sijacki et al. 2011). The infrared luminosity of CXO J101527.2+625911 calculated from IRAS ADDSCAN/SCANPI values is log ($L_{\text{FIR}} = 1.6 \times 10^{12} L_\odot$), which places this galaxy into the category of ultraluminous infrared galaxies (ULIRG: $L_{\text{FIR}} > 10^{12} L_\odot$). The high infrared luminosity supports the idea of enhanced star formation in this AGN-displaced host galaxy. The SFRs in CXO J101527.2+625911 estimated from infrared luminosity (Kennicutt & Evans 2012), 1.4 GHz radio luminosity (Murphy et al. 2011), and Hα+24 μm luminosities are 240 $M_\odot$ yr^{-1}, 387 $M_\odot$ yr^{-1} and 128 $M_\odot$ yr^{-1}, respectively. Predicted SFRs from simulations (Blecha et al. 2011; Sijacki et al. 2011) in AGN-displaced host galaxies are less well constrained and range from a few $M_\odot$ yr^{-1} to a few $\times 10^3 M_\odot$ yr^{-1}, and our estimated value fits in the middle of the predictions. However, unlike in the kinematically identified rSMBH candidates (Kim et al. 2016), we do not detect Wolf-Rayet features in the spectra, suggesting that no recent star formation activity has occurred in this galaxy. On the other hand, we find a high-excitation coronal line of [Ne V] λ3426 ($I_p = 97.11$ eV), which is an unambiguous sign of AGN activity.
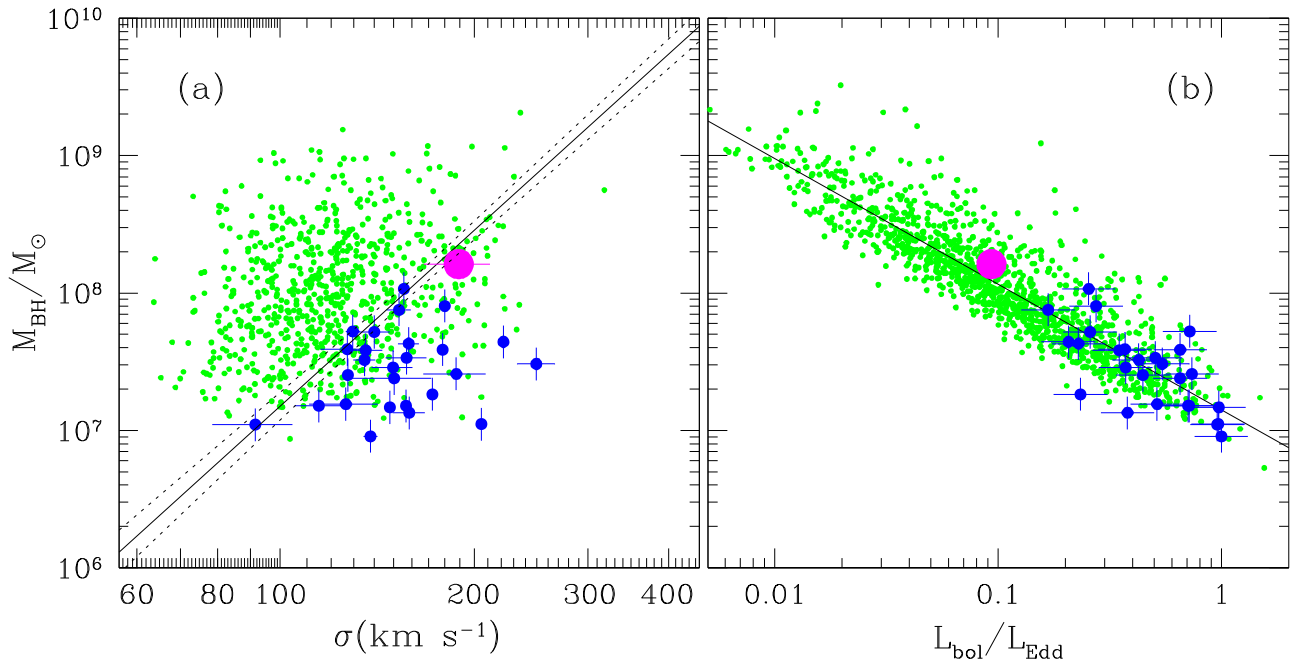
Figure 3. (a) M_{BH}–σ_* relation and (b) M_{BH} vs. Eddington ratio plots. Blue circles and green dots represent kinematically identified rSMBH candidates and their stationary counterpart of SDSS QSOs with $z < 0.25$, respectively. The solid and dotted lines in the left panel represent least-squares fits for ellipticals and classical bulges and the 1σ scatter, respectively. The solid line in the right panel represents the least-squares fit for the SDSS QSOs. The magenta circle represents the data point of CXO J101527.2+625911.

4. Summary

A systematic imaging and spectroscopic search for rSMBHs was undertaken and resulted in the detection of a potential rSMBH candidate, CXO J101527.2+625911. The following summarizes our findings:

1. A spatially offset (1.26 ± 0.05 kpc) nucleus and redshifted (175 ± 25 km s^{-1}) Hβ broad line were detected in CXO J101527.2+625911.

2. A dual SMBH scenario was investigated. The column density toward the nucleus of the host galaxy was found to be Compton thin, but no X-ray source was detected. The null detection of the SMBH in the nucleus in the *Chandra* observation suggests that either the SMBH does not exist, or that it does exist, but has a low accretion rate (LLAGN). However, the existence of an LLAGN was found to be unlikely based on the $L_{H\alpha}$, P_{radio}, and orbital velocity arguments. The X-ray and LLAGN arguments favor an rSMBH scenario.

3. The host galaxy is a bulge-dominated elliptical and shows a weak morphological disturbance in the outskirts of the galaxy, suggesting a post-merger scenario.

4. The SFRs in CXO J101527.2+625911 estimated from infrared, radio, and Hα+24 μm luminosities range from 128 $M_\odot$ yr^{-1} to 387 $M_\odot$ yr^{-1}.

5. The black hole mass ($\log M_{BH} = 8.21 \pm 0.02$ $M_\odot$) and Eddington ratio (0.09 ± 0.01) of CXO J101527.2+625911 are similar to those found in normal ellipticals. The small spatial and velocity offsets, weak morphological disturbance, elliptical galaxy type, and normal black hole mass and Eddington ratio similar to that of elliptical galaxies suggest that it has nearly completed accretion and black hole mass growth and is about to turn into a normal elliptical.

References

Andrei, A. H., Souchay, J., Zacharias, N., et al. 2009, A&A, 505, 385
Baker, J. G., Boggs, W. D., Centrella, J., et al. 2008, ApJL, 682, 29
Batcheldor, D., Robinson, A., Axon, D. J., Perlman, E. S., & Merritt, D. 2010, ApJL, 717, 6
Becker, R. H., White, R. L., & Helfand, D. J. 1995, ApJ, 450, 559
Bennert, N., Jungwiert, B., Komossa, S., Haas, M., & Chini, R. 2006, A&A, 459, 55
Blecha, L., Civano, F., Elvis, M., & Loeb, A. 2013, MNRAS, 428, 1341
Blecha, L., Cox, T. J., Loeb, A., & Hernquist, L. 2011, MNRAS, 412, 2154
Blecha, L., Sijacki, D., Kelley, L. Z., et al. 2016, MNRAS, 456, 961
Campanelli, M., Lousto, C. O., Zlochower, Y., & Merritt, D. 2007, PhRvL, 98, 231102
Civano, F., Elvis, M., Lanzuisi, G., et al. 2010, ApJ, 717, 209
Civano, F., Elvis, M., Lanzuisi, G., et al. 2012, ApJ, 752, 49
Comerford, J. M., Pooley, D., Barrows, R. S., et al. 2015, ApJ, 806, 219
Eracleous, M., Boroson, T. A., Halpern, J. P., & Liu, J. 2012, ApJS, 201, 23
Evans, I. N., Primini, F. A., Glotfelty, K. J., et al. 2010, ApJS, 189, 37
Fabian, A. C. 2012, ARA&A, 50, 455
Ferrarese, L., & Merritt, D. 2000, ApJ, 539, 9
Gebhardt, K., Bender, R., Bower, G., et al. 2000, ApJ, 539, 13

Gualandris, A., & Merritt, D. 2008, ApJ, 678, 780
Harvey, D., Massey, R., Kitching, T., et al. 2015, Sci, 347, 1462
Heckman, T. M., Lehnert, M. D., Strickland, D. K., & Armus, L. 2000, ApJS, 129, 493
Helou, G., Soifer, B. T., & Rowan-Robinson, M. 1985, ApJL, 298, 7
Ho, L. C. 2008, ARA&A, 46, 475
Ho, L. C., & Kim, M. 2015, ApJ, 809, 123
Hopkins, P. F., Hernquist, L., Cox, T. J., et al. 2005, ApJ, 630, 705
Jonker, P. G., Torres, M. A. P., Fabian, A. C., et al. 2010, MNRAS, 407, 645
Joseph, R. D., Meikle, W. P. S., Robertson, N. A., & Wright, G. S. 1984, MNRAS, 209, 111
Juneau, S., Dickinson, M., Alexander, D. M., & Salim, S. 2011, ApJ, 736, 104
Kennicutt, R. C., & Evans, N. J. 2012, ARA&A, 50, 531
Kim, D.-C., Evans, A. S., Stierwalt, S., & Privon, G. C. 2016, ApJ, 824, 122
Komossa, S., & Xu, D. 2007, ApJ, 667, 33
Komossa, S., Zhou, H., & Lu, H. 2008, ApJ, 678, 81
Kormendy, J., & Ho, L. 2013, ARA&A, 51, 511
Kormendy, J., & Richstone, D. 1995, ARA&A, 33, 581
Larson, R. B., & Tinsley, B. M. 1978, ApJ, 219, 46
Lehnert, M. D., & Heckman, T. M. 1996, ApJ, 462, 651
Lena, D., Robinson, A., Marconi, A., et al. 2014, ApJ, 795, 146
Loeb, A. 2007, PhRvL, 99, 1103
Lousto, C. O., & Zlochower, Y. 2011, PhRvL, 107, 231102
Madau, P., & Quataert, E. 2004, ApJL, 606, 17
Magorrian, J., Tremaine, S., Richstone, D., et al. 1998, AJ, 115, 2285
Marconi, A., & Hunt, L. K. 2003, ApJ, 589, 21

Menezes, R. B., Steiner, J. E., & Ricci, T. V. 2014, ApJL, 796, 13
Merritt, D., Milosavljevic, M., Favata, M., Hughes, S. A., & Holz, D. E. 2004, ApJ, 607, 9
Morić, I., Smolčić, V., Kimball, A., et al. 2010, ApJ, 724, 779
Murphy, E. J., Condon, J. J., Schinnerer, E., et al. 2011, ApJ, 737, 67
Nath, B. B., & Trentham, N. 1997, MNRAS, 291, 505
Novak, M., Smolčić, V., Civano, F., et al. 2015, MNRAS, 447, 1282
Peng, C. Y., Ho, L. C., Impey, C. D., & Rix, H.-W. 2010, AJ, 139, 2097
Peres, A. 1962, PhRv, 128, 2471
Robinson, A., Young, S., Axon, D. J., Kharb, P., & Smith, J. E. 2010, ApJL, 717, 122
Rots, A. H., & Budavári, T. 2011, ApJS, 192, 8
Rupke, D. S. N., Veilleux, S., & Sanders, D. B. 2002, ApJ, 570, 588
Sanders, D. B., Soifer, B. T., Elias, J. H., et al. 1988, ApJ, 325, 74
Scannapieco, E., Ferrara, A., & Madau, P. 2002, ApJ, 574, 590
Schnittman, J. D. 2007, ApJL, 667, 133
Shields, G. A., Rosario, D. J., Smith, K. L., et al. 2009, ApJ, 707, 936
Sijacki, D., Springel, V., & Haehnelt, M. G. 2011, MNRAS, 414, 3656
Silverman, J. D., Green, P. J., Barkhouse, W. A., et al. 2008, ApJ, 679, 118
Suh, H., Hasinger, G., Steinhardt, C., et al. 2015, ApJ, 815, 129
Tombesi, F., Melndez, M., Veilleux, S., et al. 2015, Natur, 519, 436
Tremaine, S., Gebhardt, K., Bender, R., et al. 2002, ApJ, 574, 740
Treu, T., Woo, J.-H., Malkan, M. A., & Blandford, R. D. 2007, ApJ, 667, 117
Woo, J.-H., Treu, T., Malkan, M. A., & Blandford, R. D. 2006, ApJ, 645, 900
Wrobel, J. M., Comerford, J. M., & Middelberg, E. 2014, ApJ, 782, 116